Available online at www.sciencedirect.com
SCIENCE DIRECT
Polymer 47 (2006) 1340–1347
polymer
www.elsevier.com/locate/polymer

Morphology and crystallization kinetics in a mixture of low-molecular weight aliphatic amide and polylactide

Joo Young Nam [a], Masami Okamoto [a,*], Hirotaka Okamoto [b], Mitsuru Nakano [b], Arimitsu Usuki [b], Masatoshi Matsuda [c]

[a] *Advanced Polymeric Materials Engineering, Graduate School of Engineering, Toyota Technological Institute, Hisakata 2-12-1, Tempaku, Nagoya 468 8511, Japan*
[b] *Toyota Central R&D Labs, Inc., Nagakute, Aichi 480 1192, Japan*
[c] *Toyota Motor Corporation, Susono, Sizuoka 410 1193, Japan*

Received 26 April 2005; received in revised form 15 November 2005; accepted 11 December 2005
Available online 18 January 2006

Abstract

Polylactide (PLA)/*N*,*N*-ethylenebis(12-hydroxystearamide) mixture was prepared by using melt extrusion. The detailed crystallization kinetics and morphology of neat PLA and a mixture were studied by using polarized optical microscopy, light scattering, differential scanning calorimetry, and wide-angle X-ray diffraction analyses. The overall crystallization rate and spherulitic texture of PLA were strongly influenced in presence of the organic additive. The overall crystallization rate of matrix PLA increased with addition of WX1. These behaviors indicated that WX1 crystallites, which crystallized at the very early stage of PLA crystallization act as a nucleating agent for PLA crystallization.

Keywords: Polylactide; Crystallization; Aliphatic amide

1. Introduction

Recently, demand for biodegradable polymers with excellent material properties is said to be growing with a rapid rate. In this direction, polylactide (PLA) is one of the most promising candidate because it is completely made from agricultural products and is readily biodegradable [1]. PLA is linear aliphatic thermoplastic polyester. High-molecular weight PLA is generally prepared by the ring-opening polymerization of lactide [2], which in turn is obtained by the fermentation of corn, sugar beat, etc. [1,3]. PLA has good mechanical properties, thermal plasticity and biocompatibility, and is readily fabricated, thus being a promising polymer for various end-use applications [4]. However, PLA has very bad processability because of slow crystallization rate under supercooled state.

Generally, improvement of crystallization rate of polymer can be achieved by mixing of talc that has nucleation effect in polymer matrix [5–7]. For example, Kolstad investigated the overall crystallization rate of poly(L-lactide) (PLLA) with addition of talc particles [6]. In the paper, he reported that the crystallization rates in the PLLA/talc mixture became higher than that of neat PLLA. Although the addition of an inorganic nucleating agent can be beneficial to the rate of polymer crystallization, in some cases, it should be reduce the ultimate physical properties of the material. Schmidt et al. [8] reported that crystallization rate of PLLA increased with addition of poly(D-lactide) (PDLA) because stereocomplex crystallites formed as nucleating agent in PLLA/PDLA blend.

There are many papers focusing on the nucleating effect of starch and derivatives of carboxylic and fatty acids in both PLA and biodegradable polymer matrices [9]. However, the crystallization behavior of PLLA in the presence of organic additives having low molecular weight has not been investigated sufficiently.

The relationship between structural features and crystallization kinetics in addition of organic additive is required from a fundamental viewpoint for isothermal or non-isothermal processing operations.

In this paper, we present the fine structure, morphology, and crystallization kinetics of PLA in addition of a low-molecular weight aliphatic amide as a nucleating agent. We focus on the effect of the nucleating agent in PLA matrix on the crystallization kinetics of PLA/aliphatic amide blend.

* Corresponding author. Tel.: +81 52 809 1861; fax: +81 52 809 1864.
E-mail address: okamoto@toyota-ti.ac.jp (M. Okamoto).

0032-3861/$ - see front matter © 2006 Elsevier Ltd. All rights reserved.
doi:10.1016/j.polymer.2005.12.066

2. Experimental

2.1. Materials

PLA with D content of 0.8% was supplied from Toyota Motor Corporation and dried under vacuum at 80 °C for 48 h and then kept under a dry nitrogen atmosphere prior to use. *N*,*N*-Ethylenebis(12-hydroxystearamide) (WX1; Kawaken Fine Chemical Co., Ltd melting temperature (T_m) = 144.5 °C) was prepared as a nucleating agent (see chemical structure). The mixture of WX1 and PLA was melt extruded using a twin-screw extruder (TEX30α, The Japan Steel Works, Ltd) operated at 200 °C (screw speed = 300 rpm, feed rate = 120 g/min) to yield blend strands (denoted as PLAWX1 including 1 wt% of WX1). The strands were pelletized and dried under vacuum at 60 °C for 48 h to remove water completely. The additive appears not to be soluble in PLA, suggesting no interaction of the two secondary alcohols on the compound with PLA (alcoholysis). For this reason, we do not take into account a potential of plasticization of the PLA matrix by the low-molar mass additive.

C_6H_{13}–C(OH)H–$C_{10}H_{20}$–CONH–C_2H_4

–NHCO–$C_{10}H_{20}$–C(OH)H–C_6H_{13}

Chemical structure of WX1

2.2. Gel permeation chromatography (GPC)

The weight-average (M_w) and number-average (M_n) molecular weights of PLA and matrix PLA in PLAWX1 were determined from GPC (LC-VP, Shimadzu Co.), using polystyrene standards for calibration and tetrahydrofuran (THF) as the carrier solvent at 40 °C with a flow rate of 0.5 mL/min. For the GPC measurements first PLA or PLAWX1 were dissolved in chloroform and then diluted with THF. The GPC results are presented in Table 1.

As anticipated, the incorporation of WX1 resulted in a reduction in the molecular weight of the PLA matrix. Decreased molecular weights of PLA in PLAWX1 may be explained by either the shear mixing of PLA and WX1, resulting in a certain degree of hydrolysis of PLA matrix at high temperature.

2.3. Crystallization

The thin film (ca. 30 μm thick) was prepared by pressing the film between two cover glasses at 200 °C. After the specimen was held at 200 °C for 5 min, it was rapidly transferred into a hot stage (Linkam, Linkam Scientific instruments, Ltd) set at the desired crystallization temperature. The temperature in Linkam hot stage was calibrated with Indium before use. The morphology and spherulitic growth behavior of neat PLA and PLAWX1 films were measured by using light scattering (LS) and polarized optical microscopy (POM) (Nikon OPTI-PHOTO2-POL). The thick film (ca. 1 mm) was also prepared by pressing and then crystallized by the above method. The crystallized specimens were characterized by using differential scanning calorimeter (DSC) and wide angle X-ray diffraction (WAXD).

Table 1
Characteristics parameters of neat PLA and PLAWX1

Parameters	Neat PLA	PLAWX1
$M_w \times 10^{-3}$ (g mol^{-1})	102	99.5
M_w/M_n	2.71	2.14
T_m (°C)	174.1	173.5
T_g (°C)	54	52
T_{cc} (°C)	100.7	79.7

2.4. Light scattering (LS)

A polarized He–Ne laser of 632.8 nm wavelength was applied vertically to the film specimen. The angular distribution of the light scattering intensity was detected by a highly sensitive photodiode sensor. We employed the Hv geometry in which the optical axis of the analyzer was set perpendicularly to that of the polarizer. The input data from the photodiode sensor was digitized by the controller. The digitized data were stored in a personal computer for further analysis [5].

2.5. WAXD

WAXD analyses were performed for WX1 and PLAWX1 on a Mxlabo diffractometer (MAC Science Co.; 3 kW, graphite monochromator, Cu Kα radiation (λ_x = 0.154 nm), operated at 40 kV and 20 mA). Samples were scanned in fixed time mode with counting time of 2 s under diffraction angle 2θ in the range of 5–40°.

2.6. Differential scanning calorimeter

The crystallized specimens were characterized by using temperature-modulated DSC (TA 2920; TA Instruments) at the heating rate of 5 °C/min with a heating/cooling cycle of the modulation period of 60 s and an amplitude of ±0.769 °C, to determine the glass transition (T_g) crystallization temperature (T_{cc}) and the melting temperature (T_m). The DSC was calibrated with indium before use. The obtained values are also presented in Table 1. For the measurement of T_{cc}, we used amorphous samples after quenching from malt state (~200 °C).

2.7. TEM

Nanoscale structure of WX1 was investigated by means of TEM (H-7100, Hitachi Co.), operating at an accelerating voltage of 100 kV. The ultra thin section (the edge of the sample sheet perpendicular to the compression mold) with a thickness of 100 nm was microtomed by using a Reichert Ultra cut cryo-ultramicrotome with RuO_4 staining.

3. Results and discussion

3.1. Morphology of WX1

Fig. 1(a) shows POM picture of WX1 after crystallization at 110 °C for 10 min. The spherulitic texture of WX1 is very quickly formed during isothermal crystallization. The spherulites exhibited the negative birefringence. This spherulitic texture is confirmed by LS pattern under Hv mode. As show in Fig. 1(b), four-leaf-clover type pattern was observed in the crystallized WX1. The results suggest that spherulites are formed and crystallites are arranged along the radial direction within the spherulite [10].

Fig. 2 shows TEM picture of the crystallized WX1 at 110 °C for 10 min. The fine structure within the spherulite of WX1 exhibited lamella structure. Here, we should mention that spherulitic texture and lamella structure is generally formed during the crystallization of polymer. Hence the WX1 crystallites having the spherulitic texture similarly to that of polymer may easily act as a nucleating agent for PLA crystallization.

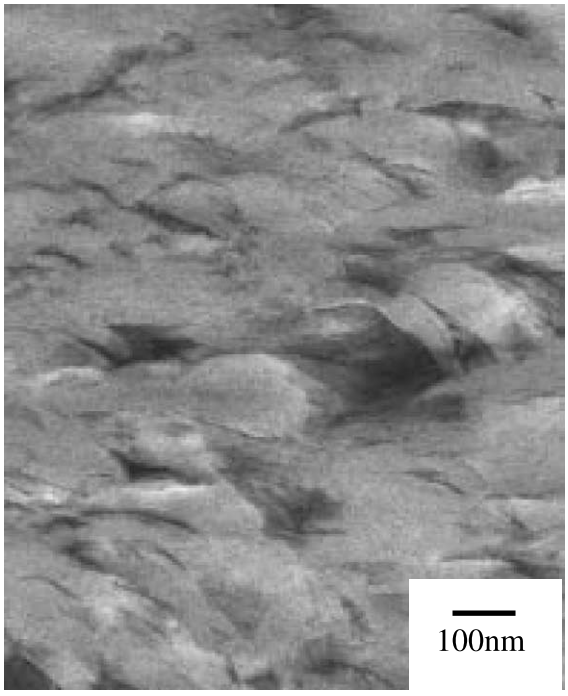

Fig. 2. High-resolution TEM image of WX1 crystallized at $T_c = 110$ °C for 10 min.

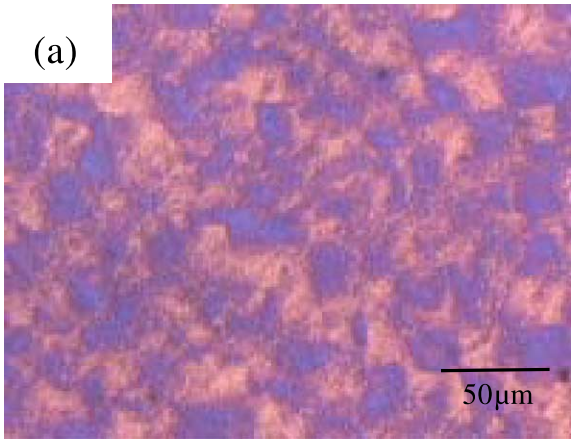

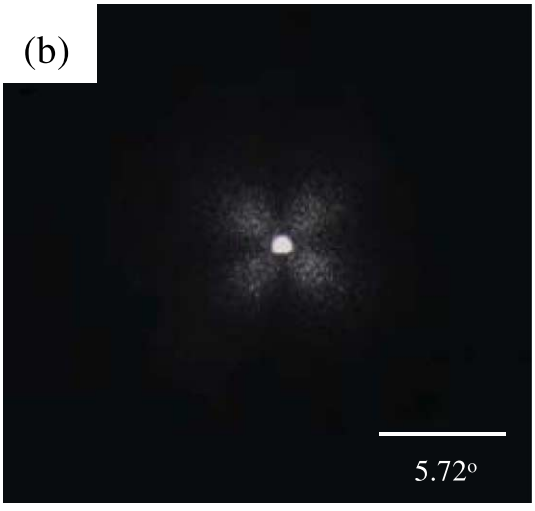

Fig. 1. (a) Optical micrographs and (b) Hv light scattering patterns of WX1 at $T_c = 110$ °C for 10 min.

3.2. Transcrystallization at interface between PLA and WX1

Generally, in fiber-reinforced polymer, the fibers induce a relatively high crystal nucleation density on their surface under certain conditions. Therefore, the matrix spherulites grow in the radial direction of the fiber, to produce a cylindrical layer of crystallite, termed transcrystallite. In order to investigate the nucleation effect of WX1, we observed at interface between PLA and WX1. In Fig. 3, typical transcrystallites at the interface are observed. The well-developed layer of transcrystallite grown from WX1 surface is the evidence of the epitaxial crystallization of PLA in the presence of WX1. Without epitaxial growth the nucleation effect does not appear in the mixture of polymer and additive.

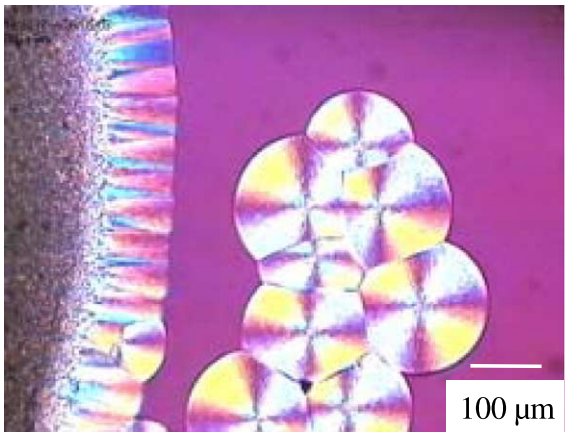

Fig. 3. Optical micrographs at interface between PLA and WX1 at $T_c = 130$ °C for 30 min.

3.3. Nucleation effect of WX1 during isothermal crystallization

In order to develop the nucleation effect, the finely dispersed WX1 in PLA matrix must be crystallized at early stage of the PLA crystallization. Fig. 4 shows WAXD profiles of neat PLA and PLAWX1 after quenching from melt state (~200 °C). Despite quenching from melt, the pure WX1 exhibits a very strong reflection peak as shown in Fig. 4(a). We can recognize that the crystallization rate of pure WX1 is very fast. Fig. 4(b) shows the corresponding WAXD profile of PLAWX1 from melt. As seen in the figure, the result exhibits a liquid-like halo along with small peaks (shown by the arrows). The unit cell geometry of pure WX1 is not clear at present, however, we note that the dispersed WX1 can crystallize well in PLA matrix during rapid quenching and then the dispersed and crystallized WX1 domains act as a nucleating agent of PLA crystallization.

3.4. Nucleation effect of WX1 with crystallization temperature

The spherulitic texture was observed by POM. Optical micrographs of neat PLA (a–c) and PLAWX1 (a′–c′) with isothermal crystallization temperature (T_c) for 1.5 h are shown in Fig. 5. As shown in Fig. 5, the spherulites are formed after the isothermal crystallization both neat PLA and PLAWX1. These spherulites exhibited negative birefringence and higher ordered spherulitic texture [11]. The decrease in spherulite size with addition of WX1 is clearly observed at $T_c = 110$ and 130 °C for 1.5 h. However, the spherulite size at $T_c = 150$ °C is not change with addition of WX1. Here, it should be mentioned that T_m of pure WX1 is 144.5 °C. This suggests that the finely dispersed WX1 in PLAWX1 is not able to crystallize at $T_c =$ 150 °C. Thus, the spherulite size is not change at higher T_c (> 145 °C) due to no nucleation effect of the dispersed WX1. This is confirmed by WAXD experiment. The WAXD profiles of neat PLA and PLAWX1 crystallized at $T_c = 100$ and 150 °C for 1.5 h are shown in Fig. 6. As show in Fig. 6, the neat PLA and the crystallized PLAWX1 at 150 °C exhibit a very strong reflection at $2\Theta = 17.1°$ due to diffraction from (200) and/or (110) planes and another reflection peak at $2\Theta = 19.5°$ occurring from (203) plane. These profiles indicate that neat PLA crystals are the typical orthorhombic crystal [11,12]. However, in the case of the PLAWX1 crystallized at 100 °C, these peaks are shifted towards lower diffraction angle and another reflection peak at $2\Theta = 5.8°$ appears due to the crystallization of WX1. Hence PLAWX1 sample crystallized in defect ridden crystalline form due to the nucleation accompanied with WX1 crystallites. This suggests that the nucleation effect of WX1 does not appear above T_m of pure WX1 as mentioned before.

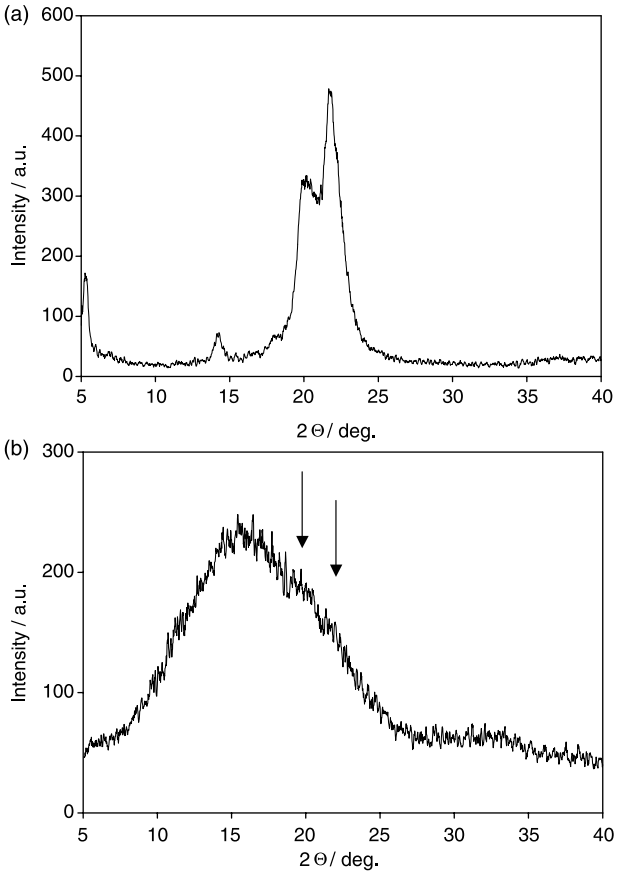

Fig. 4. Typical WAXD profiles of (a) WX1 and (b) PLAWX1 samples quenched from melt.

3.5. Spherulite radius and nucleation density of PLAWX1

At low T_c (≤120 °C), as the size of the spherulites are small, i.e. out of range for the POM experiment, we observed them by using light scattering method. Fig. 7 shows the change in the Hv light scattering patterns after the isothermal crystallization of neat PLA ((a)–(c)) and PLAWX1 ((a′)–(c′)) at $T_c = 100$–120 °C for 3 h. Four-leaf-clover type pattern was observed under Hv mode for neat PLA and PLAWX1 at all of the T_c after crystallization. The one-dimensional Hv scattering profiles at an azimuthal angle of 45° in the scattering patterns of Fig. 7 has a maximum at scattering angle θ_m. The θ_m is related to the average radius of the spherulite R_s [10]:

$$4.09 = 4\pi \frac{R_s}{\lambda} \sin \frac{\theta_m}{2} \quad (1)$$

where λ is the wavelength of the He–Ne laser.

Hence, the θ_m is expected to become smaller when the R_s become larger. As shown in Fig. 8(a), the R_s calculated from a maximum scattering angle become smaller with addition of WX1 at any crystallization temperatures. This shows that the dispersed WX1 act as a nucleating agent, which is evident from the increase in the number of nuclei causing smaller spherulites formation.

From Fig. 8(a), the number of heterogeneous nuclei can be estimated from a rough approximation. That is, all the spherulites were of identical size, the primary nucleation density of the spherulites, i.e. the number of heterogeneous nuclei N, was estimated by [13]:

$$N = \frac{3}{4\pi} R_m^{-3} \quad (2)$$

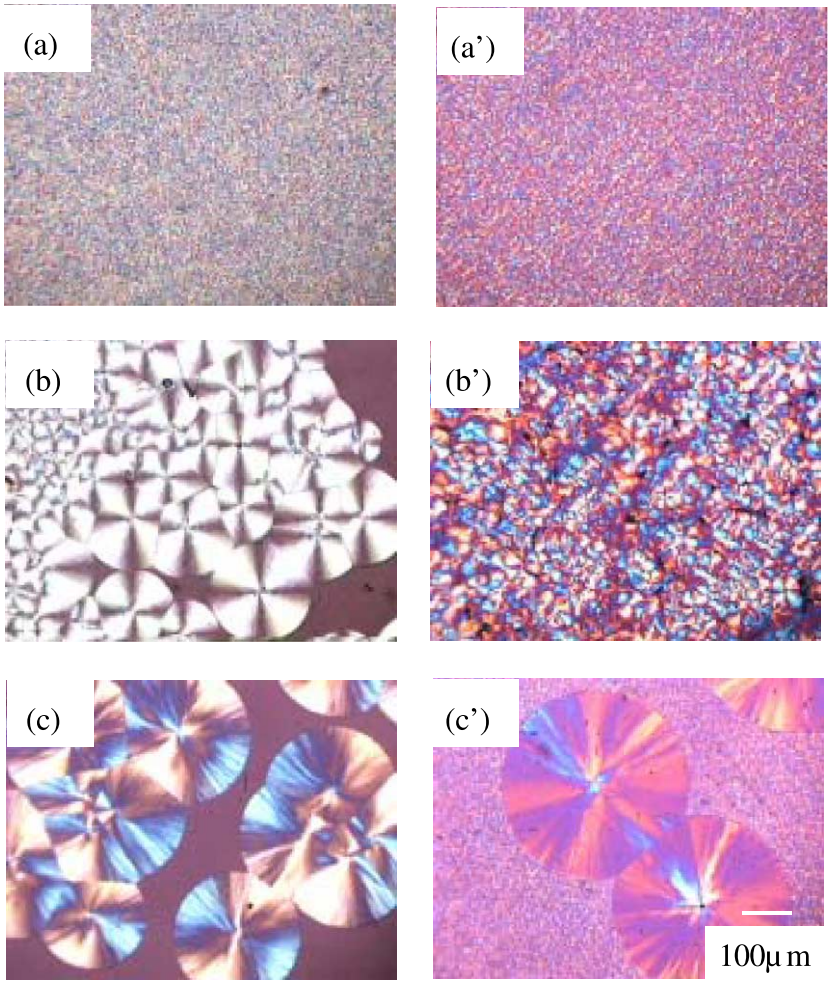

Fig. 5. Optical micrographs of neat PLA (a–c) and PLAWX1 (a′–c′) at various crystallization temperature T_c for 1.5 h: (a, a′) $T_c = 110$ °C; (b, b′) $T_c = 130$ °C; (c, c′) $T_c = 150$ °C.

where R_m is the maximum radius of the spherulite ($\equiv R_s$), i.e. the attainable radius before impingement. The calculated value of N is shown in Fig. 8(b). The N value at 130 °C was 3.24×10^{-7} μm^{-3} for neat PLA and 121×10^{-7} μm^{-3} for PLAWX1. The time variation of the volume fraction of the spherulites increases in proportion to NG^3 ($\cong$overall crystallization rate), G is the radial growth rate of the spherulite. This fact suggests that the overall crystallization rates of the PLAWX1 at high temperature ($T_c = 130$ °C) are about two orders of magnitude higher than that of matrix PLA without WX1 if G value for PLAWX1 is not so different from that for neat PLA.

The difference of N between neat PLA and PLAWX1 at $T_c = 130$ °C is higher than that at low T_c. This suggests that the PLAWX1 exhibits a heterogeneous nucleation kinetics, which depends on more originating from the well-dispersed WX1 crystallites at high T_c.

3.6. Crystallization kinetics

To understand the crystallization kinetics of neat PLA and PLAWX1 at low T_c (≤ 130 °C), we have used time-resolved LS photometry, which is a powerful tool for estimating the overall crystallization rate and its kinetics in supercooled crystalline polymer liquid [14]. For the kinetics of crystallization, we can employ the integrated scattering intensity, i.e. the invariant Q is define as

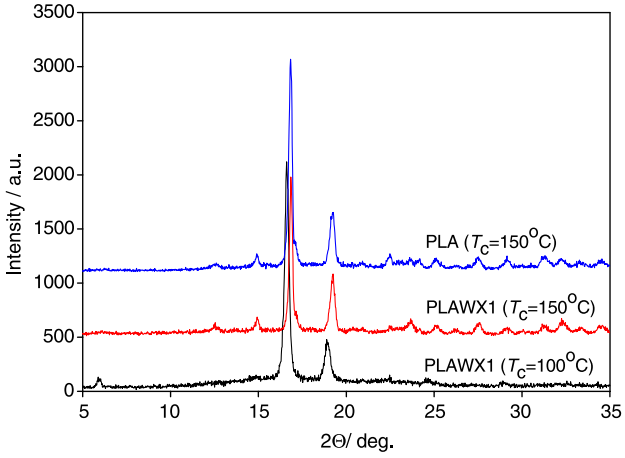

Fig. 6. Typical WAXD profiles of neat PLA and PLAWX1 samples crystallized at 100 and 150 °C for 1.5 h.

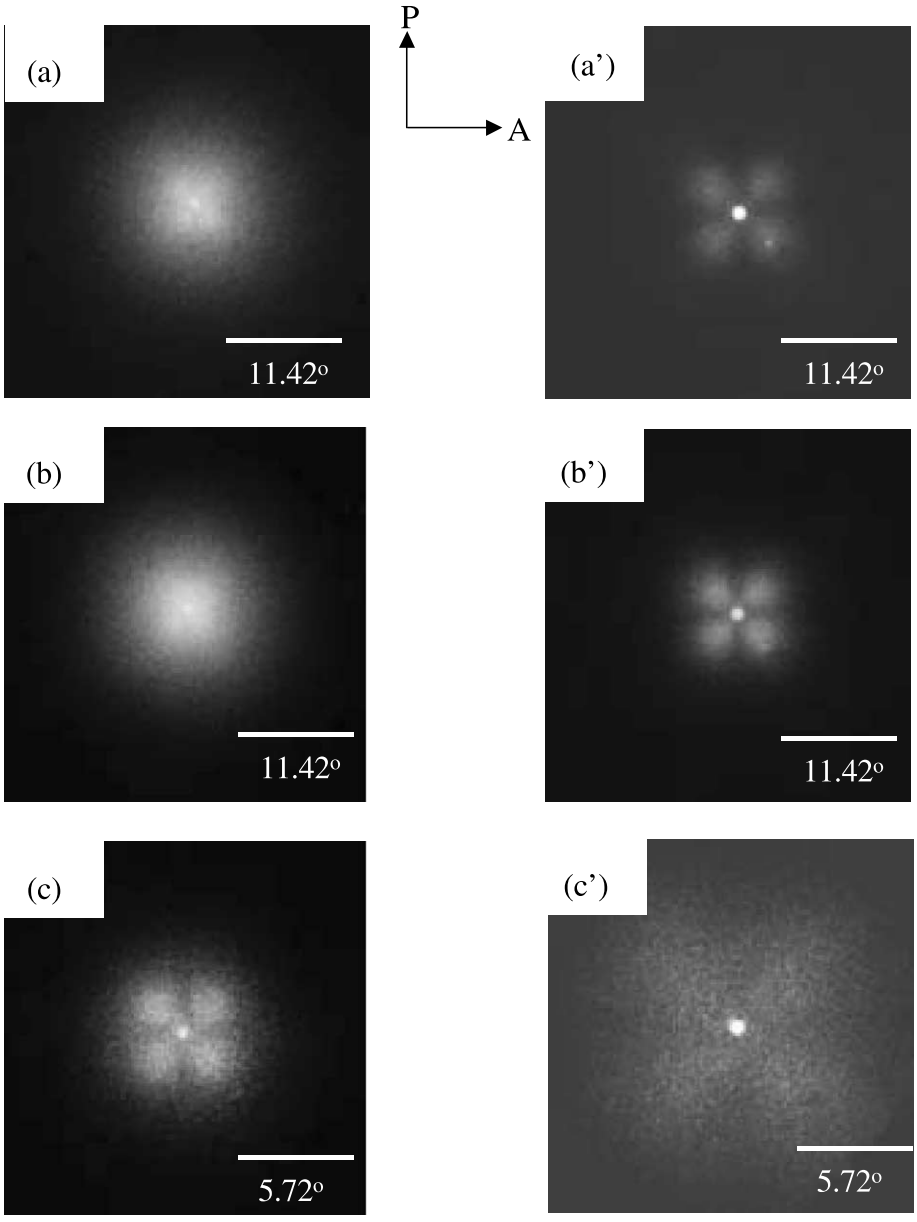

Fig. 7. Changes in Hv light scattering patterns of neat PLA (a–c) and PLAWX1 (a′–c′) at various crystallization temperature under Hv modes: (a, a′) $T_c = 100$ °C; (b, b′) $T_c = 110$ °C; (c, c′) $T_c = 120$ °C for 3 h.

$$Q = \int_0^\infty I(q) q^2 \mathrm{d}q \tag{3}$$

where q is the scattering vector ($=(4\pi/\lambda_{LS})\sin(\Theta_{LS}/2)$), λ_{LS} is the wavelength of light in the specimen, Θ_{LS} is the scattering angle, and $I(q)$ is the intensity of the scattered light at q, respectively [15].

In the Hv mode, the invariant Q_δ can be described by the mean-square optical anisotropy $\langle\delta^2\rangle$:

$$Q_\delta \propto \langle\delta^2\rangle \propto \phi_s(\alpha_r - \alpha_t)^2 \tag{4}$$

where ϕ_s is the volume fraction of spherulites, and α_r and α_t are the radial and tangential polarizabilities of spherulites, respectively. We constructed a plot of reduced invariant Q_δ/Q_δ^∞ vs time t with Q_δ^∞ being Q_δ at an infinitely long time of crystallization (up to full solidification of the melt).

Fig. 9 shows the time variation of the invariant Q_δ/Q_δ^∞ taken for neat PLA and PLAWX1 at 110 °C. The overall crystallization rate was determined from the slope $Q_\delta/Q_\delta^\infty(\mathrm{d}(Q_\delta/Q_\delta^\infty)/\mathrm{d}t)$ in the crystallization region as indicated by the solid line in Fig. 9, and we plotted it in Fig. 10. It is clear that the overall crystallization rate increases in PLAWX1 compared to the pristine PLA at wide range of T_c studied here. The overall crystallization rate against T_c plots are a typical ordinal rate curve for semicrystalline polymers [16]. However, the rate of PLAWX1 is enhanced for every temperature of measurement, especially at lower T_cs, which can explain well the plot of induction time against T_c. From the onset time (t_0), we can estimate the induction time of the crystallization until start of

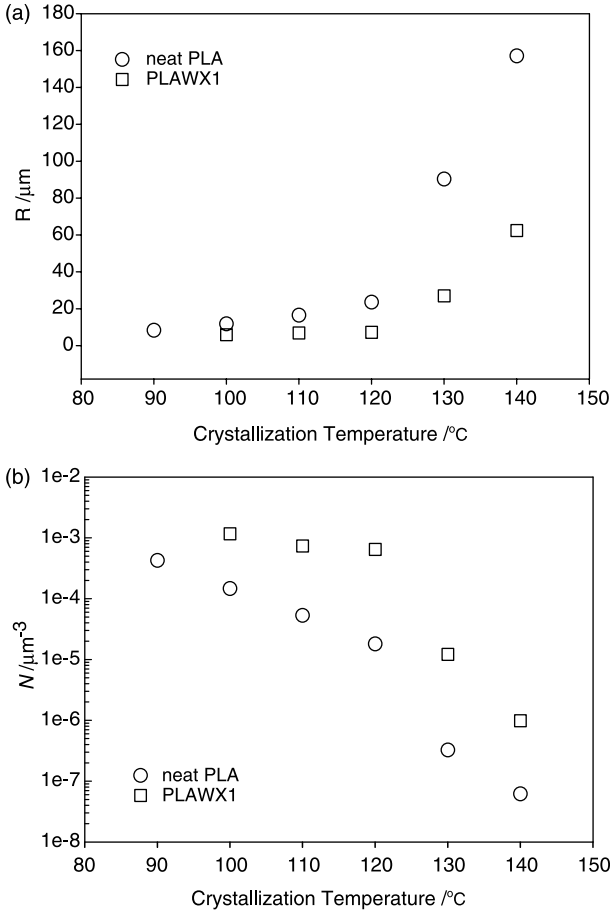

Fig. 8. (a) Spherulite radius, R, and (b) nucleation density, N, of neat PLA and PLAWX1 as a function of T_c.

crystallization. The value of t_0 in PLAWX1 estimated from any T_c become faster than that of PLA without WX1, especially at lower T_cs as well as crystallization rate. The enhancement of overall crystallization rate is accomplished by this fast nucleation rate (Fig. 11).

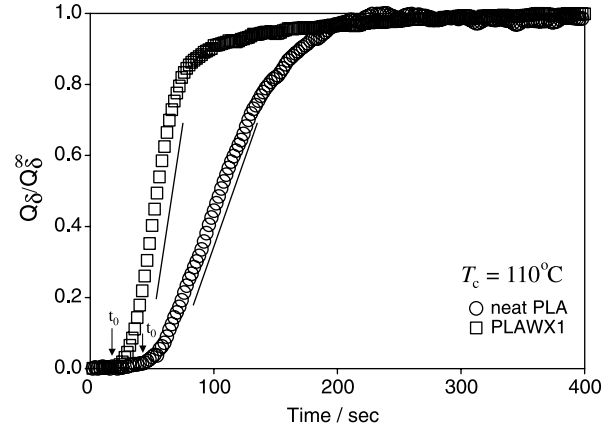

Fig. 9. Time variation of reduced invariant Q_δ/Q_δ^∞ during isothermal crystallization at quiescent state at $T_c = 110$ °C. The solid line represents the slope (overall crystallization rate).

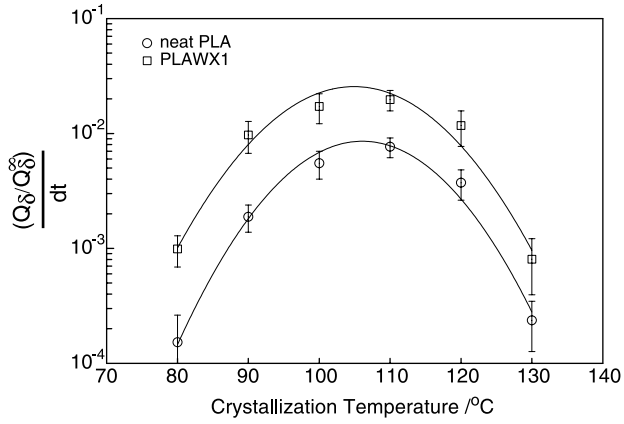

Fig. 10. T_c dependence of the overall crystallization rate of neat PLA and PLAWX1.

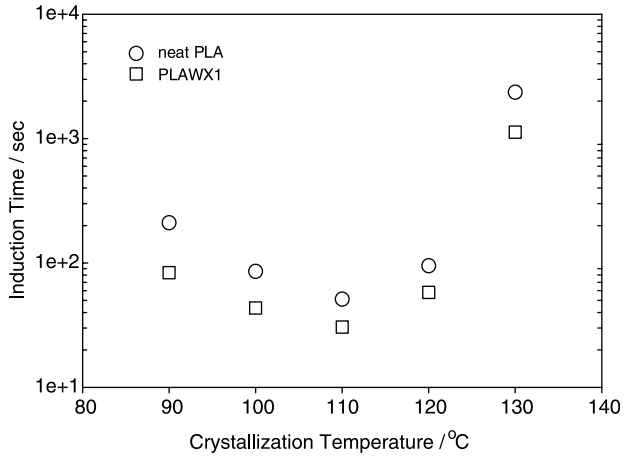

Fig. 11. T_c dependence of the induction time, t_0, of neat PLA and PLAWX1.

4. Conclusions

In this paper, we described the detail crystallization behavior and morphology of neat PLA and PLAWX1. The morphology of pure WX1 after crystallization exhibited the spherulitic texture and lamella structure. Both neat PLA and PLAWX1 spherulites showed negative birefringence. Incorporation of WX1, a typical tanscrystallition occurred at the interface between PLA and WX1 due to the nucleation effect of WX1. The overall crystallization rate of matrix PLA increase with addition of WX1. These behaviors indicate that WX1 crystallites, which crystallized at the very early stage of PLA crystallization act as a nucleating agent for PLA crystallization.

References

[1] Drumright RE, Gruber PR, Henton DE. Adv Mater 2000;12:1841.
[2] (a) Kim SH, Han Y-K, Kim YH, Hong SI. Macromol Chem 1991;193:1623.
(b) Kricheldorf HR, Serra A. Polym Bull 1985;14:497.
(c) Kricheldorf HR, Berl M, Scharngal N. Macromolecules 1988;21:286.
(d) Nijenhuis AJ, Grijpma DW, Pennings AJ. Macromolecules 1992;25:6419.

[3] Lunt J. Polym Degrad Stab 1998;59:145.
[4] (a) Grijpma DW, Pennings AJ. Macromol Chem Phys 1994;195:1649.
(b) Perego G, Cella GD, Bastioli C. J Appl Polym Sci 1996;59:37.
(c) Sinclair RG. J Macromol Sci, Pure Appl Chem 1996;A33:585.
(d) Tsuji H, Ikada Y. J Appl Polym Sci 1998;67:405.
(e) Martin O, Averous L. Polymer 2001;42:6209.
[5] Okamoto M, Shinoda Y, Kinami N, Okuyama T. J Appl Polym Sci 1995; 57:1055.
[6] Kolstad JJ. J Appl Polym Sci 1996;62:1079.
[7] Haubrug HG, Daussin R, Jonas AM, Legras R. Macromolecules 2003;36: 4452.
[8] Schmidt SC, Hillmyer MA. J Polym Sci, Polym Phys 2001;39:300.
[9] (a) Martin O, Averous L. Polymer 2001;42:6209.
(b) Ke T, Sun X. J Appl Polym Sci 2003;89:1203.
(c) Nippon catalytic chemistry and industry, US Patent 6,521,717; 2003.
[10] Stein RS, Rhodes MB. J Appl Phys 1960;31:1873.
[11] (a) Eling B, Gogolewski S, Pennings AJ. Polymer 1982;23:1587.
(b) Vasanthakumari R, Pennings AJ. Polymer 1983;24:175.
[12] (a) Hoogsteen W, Postema AR, Pennings AJ, TenBrinke G, Zugenmaier P. Macromolecules 1990;23:634.
(b) Kobayashi J, Asahi T, Ichiki M, Okikawa A, Suzuki H, Watanabe T, et al. J Appl Phys 1995;77:2957.
(c) Brizzolara D, Cantow HJ, Diederichs K, Keller E, Domg AJ. Macromolecules 1996;29:191.
[13] Maiti M, Nam PH, Okamoto M, Hasegawa N, Usuki A. Macromolecules 2002;35:2042.
[14] Kubo H, Sato H, Okamoto M, Kotaka T. Polymer 1998;39:501.
[15] Okamoto M, Inoue T. Polymer 1995;36:2736.
[16] Moore Jr EP. Polypropylene handbook. Cincinnati, OH: Hanser/Gardner; 1996.